RSC Advances

ROYAL SOCIETY OF CHEMISTRY

www.rsc.org/advances

Journal Name

ARTICLE

Comparison of Sandwich and Fingers-crossing Type $WO_3/BiVO_4$ Multilayer Heterojunctions for Photoelectrochemical Water Oxidation

Received 00th January 20xx,
Accepted 00th January 20xx

DOI: 10.1039/x0xx00000x

www.rsc.org/

Cong Liu, Jinzhan Su* and Liejin Guo

WO_3 and $BiVO_4$ thin films were spincoated on FTO in a intersected way with WO_3 and $BiVO_4$ overlapped only in the center part, resulting in multilayer fingers-crossing thin films (fingers-crossing heterojunction). Samples with only overlapped area (sandwich heterojunction) were obtained by cutting off the un-overlapped area of both WO_3 and $BiVO_4$ layers (node) as a counterpart for comparison. The influences of layer number, layer thickness and junction type on the photoelectrochemical (PEC) water splitting performance under simulated solar light for the obtained heterojunctions were investigated. XRD, SEM, XPS and Uv-vis absorption measurements were conducted to investigate its structural properties and morphology. The photocurrent density of sandwich heterojunction is higher than that of fingers-crossing heterojunction at low applied bias. The IPCE shows that both fingers-crossing heterojunction and sandwich heterojunction can utilize effectively light up to 510 nm. Mott-schottky plots shows that the sandwich heterojunction has a more negative flat band potential, which is desirable for water splitting, than fingers-crossing heterojunction. In addition, the mechanism of photogenerated carriers separation in these two heterojunctions was discussed.

1 Introduction

Photoelectrochemical (PEC) water splitting for hydrogen production has been considered as one of the most promising artificial photosynthesis[1] to utilize solar energy and address critical energy security and environmental sustainability issues.[2-5] Although many semiconductor materials such as TiO_2, ZnO, Fe_2O_3, CdS, $SrTiO_3$[6-9] have been reported to be effective for PEC hydrogen production, most of them are limited in utilization due to serious photocorrosion, high charge carrier recombination, or large band gap[10]. In order to take full advantage of each material merits and avoid their weakness, many composite semiconductor materials such as Si/Fe_2O_3[11], TiO_2/CdS[12], ZnO/CdS[13], $BiVO_4/TiO_2$[14], $BiVO_4/ZnO$[15], WO_3/Fe_2O_3[16] have been designed and tested to address those issues. In a typical semiconductor heterojunction with type II band alignment, photogenerated electron-hole pairs tend to be spatially separated on different sides of the heterojunction, achieving efficiently photogenerated electron-hole pair separation [17, 18].

Recently, $BiVO_4$ photoelectrodes have emerged as a popular semiconductor for photoelectrochemical application and attracted considerable attention[19-24]. The $BiVO_4$ owing to its band gap of 2.4eV (monoclinic) is capable of sufficiently absorbing the solar spectrum and stable against photocorrosion in an aqueous electrolyte with mild pH (between 3 and 11)[25-27], but unfortunately its charge carrier recombination rate is relatively high[4, 21]. In order to improve the charge carrier separation in $BiVO_4$, combining with other semiconductor with a suitable band gap energy level and good carrier mobility have been adopted. For example, WO_3 conduction band (CB) level is more positive than that of $BiVO_4$ and possesses a good carrier mobility[18, 28, 29]. Many types of $WO_3/BiVO_4$ heterojunctions were fabricated in past five years. For example, Jae Sung Lee et al.[30] fabricated the flat $WO_3/BiVO_4$ heterojunction photoelectrodes on FTO with the $BiVO_4$ layers optimized. Hyeok Park et al.[31] fabricated the WO_3/Mo-$BiVO_4$ heterojunction photoelectrodes by atomic doping. Ligang Xia et al.[32] fabricated $BiVO_4/WO_3$/W heterojunction photoanode on the nanoporous WO_3 film. Core/shell $WO_3/BiVO_4$ nanowire and nanorod photoanodes were fabricated by Zheng et al.[33] and Pihosh et al.[34] respectively. To further improve the PEC performance of the $WO_3/BiVO_4$ heterojunction, cobalt phosphate (Co-Pi)[29, 34, 35], FeOOH[36] and NiOOH[36, 37] oxygen evolution catalysts (OECs) were deposited on the $WO_3/BiVO_4$ heterojunction through different technologies. The dynamics of photogenerated charge carriers in $WO_3/BiVO_4$ heterojunction photoanodes was also studied by Ivan Grigiono and his co-workers[38]. In our previous study[10, 39], nanostructural $WO_3/BiVO_4$ heterojunction with efficient carrier separation was realized. It is desirable to further study this efficient heterojunction to maximize the ability of charge separation in the heterojunction.

International Research Centre for Renewable Energy, State Key Laboratory of Multiphase Flow in Power Engineering, Xi'an Jiaotong University, Shaanxi 710049, P. R. China. E-mail: j.su@mail.xjtu.edu.cn.

† Electronic Supplementary Information (ESI) available: XRD of multilayer heterojunctions (Fig.S1), optical behavior of heterojunctions (Fig.S2), photocurrent density of heterojunctions (Fig.S3). See DOI: 10.1039/x0xx00000x

However, most reported WO_3/$BiVO_4$ heterojunctions are single heterojunction which yet don't have efficient light absorption or charge transfer. Fatwa F. Abdi et al.[40] reported a charge carrier diffusion length of 70nm for $BiVO_4$. Reducing the thickness of $BiVO_4$ layers could be a solution but its light absorbance is insufficient. Using multilayer heterojunctions may avoid these deficiencies via controlling the layer thickness and layer number.

In this study, we fabricated fingers-crossing and sandwich type multilayer heterojunction photoelectrodes and compared their PEC performance to investigate the junction type effect on PEC water oxidation. Although the maximum photocurrent of the films is much less than the recent record value of core-shell WO_3/$BiVO_4$ nanorods (6.72 mA/cm^2 at 1.23 V_{RHE}) reported by Pihosh and his co-workers[34], the effect of heterojunction structure including layer numbers and connecting way on its performance is rarely investigated. So we tried to discuss the carrier separation in these two types of multilayer heterojunction, and investigated the influences of layer number and layer thickness on PEC performances. At last a possible mechanism for the influences of junction node on PEC water splitting was proposed.

2 Experimental

2.1 Film preparation

For WO_3 precursor solution (0.125M), 0.01mol Tungsten acid (H_2WO_4) and 25 ml H_2O_2 (30 wt.%) were dissolved in 15 ml de-ionized water (H_2O) then mixture with 40 ml PVA (poly vinyl alcohol) precursor solution (0.5 g PVA dissolved in 10 ml H_2O). For $BiVO_4$ precursor solution (0.125M), 0.01mol $Bi(NO_3)_3{\cdot}5H_2O$, 0.01mol NH_4VO_3 and 10 ml concentrated nitric acid (HNO_3) were dissolved in 30 ml de-ionized water then mixture with 40 ml PVA solution. Fluorine-doped SnO_2 (F:SnO_2, FTO)-coated glass substrates (TEC-15, 15 Ω/sq) were cleaned by successive ultrasonic cleaning in acetone, de-ionized water and ethanol for 30 min, and then dried in nitrogen flow. Intersected overlapped WO_3 and $BiVO_4$ was synthesized on FTO substrates by spin-coating of WO_3 and $BiVO_4$ layer by layer, the spin rate was controlled in 3000 rpm for 30s. For fingers-crossing heterojunction, each layer covered undesired part via scotch tape was coated on the top of previous layers after calcinations (500 ℃/2h) between coatings. For sandwich heterojunction, cut off both WO_3 node and $BiVO_4$ node of fingers-crossing heterojunction.

2.2 Film characterizations

Employ X'pert PRO diffractormeter (PANalytical, using Cu Ka irradiation, λ=15.4184 nm) in performing X-ray diffraction (XRD) analysis and determining the structure and phase of the samples. Employ JSM-7800FE instrument (JEOL) in performing field emission scanning electron microscopy (FE-SEM). Employ X-ray photoelectron spectroscopy (XPS, Axis UltraDLD, Kratos) with monochromatic aluminum K α radiation obtaining atomic ratio of samples by etching. Employ Hitachi U-4100 UV-vis-NIR spectrophotometer equipment in recording optical UV–vis absorption spectra of the samples.

2.3 Photoelectrochemical measurements

The PEC measurements were performed by a scanning potentiostat (CH Instruments, model CHI 760D) using a standard three-electrode system in 0.5 M Na_2SO_4 as electrolyte with Ag/AgCl, Pt plate as reference electrode, counter electrodes, respectively. The applied bias was converted to the value against a reversible hydrogen electrode (RHE) by using the equation (1) below.

$$E_{RHE} = E_{Ag/AgCl} + E^0_{Ag/AgCl} + 0.0591\ V \times pH \quad (1)$$
$$(E^0_{Ag/AgCl} = 0.1976\ \text{V vs. NHE at 25 ℃})$$

The simulated solar spectrum generated by a fiber optic spectrometer (AvaSpec-2048) using 350 W xenon lamps set 100mW/cm^2 as light source. The electrochemical impedance spectroscopy (EIS) was performed at 1.1 V_{RHE} with a frequency of 100 kHz-1 Hz under illumination. Apart from above, a Newport monochromator 74126 and a burning glass made of quartz were used to measure incident photon to current conversion efficiency (IPCE).

3 Results and discussion

To compare the PEC performances of sandwich heterojunction and fingers-crossing heterojunction, we prepared bare WO_3, fingers-crossing/sandwich WO_3-$BiVO_4$-n (n = 1, 2, 3, 4, 5) heterojunctions and bare $BiVO_4$ photoelectrodes via spin-coating method. The number n is denoting the repeat number of WO_3/$BiVO_4$ layers in fingers-crossing or sandwich heterojunctions. Sandwich heterojunction photoelectrodes were made by cutting off the WO_3 node and $BiVO_4$ node area of fingers-crossing heterojunction with only multijunction area left to form clean cross sections. All WO_3 and $BiVO_4$ layers were prepared with same condition. The configuration of samples is represented in Scheme 1.

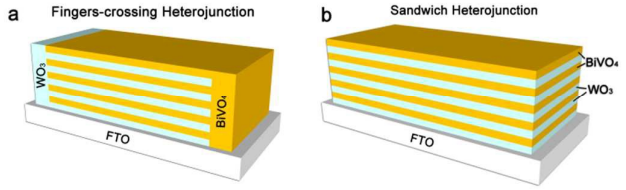

Scheme 1 Geometric illustration of finger-crossing heterojunction and sandwich heterojunction. The yellow layer represents $BiVO_4$ and light blue layer stands for WO_3.

3.1 Structure and morphology

The crystal structures of the bare film or heterojunctions were examined by XRD analysis. For comparison, the XRD pattern obtained from FTO is also shown in Fig.1. The XRD patterns of all photoelectrodes exhibited strong peaks corresponding to FTO on the substrate. The crystal phase of the bare WO_3 photoelectrode was identified to be monoclinic (JCPDS Card No. 01-071-2141). The bare $BiVO_4$ photoelectrode exhibited a monoclinic scheelite type crystal structure (JCPDS Card No. 00-014-0688). For the WO_3-$BiVO_4$-n (n=1, 2, 3, 4, 5) photoelectrodes, the exhibited peaks corresponding to WO_3 and $BiVO_4$ indicates the absence of any new compound

formation. The X-Ray diffraction patterns of WO_3-$BiVO_4$-n (n=2, 4) were shown in Fig.S1.

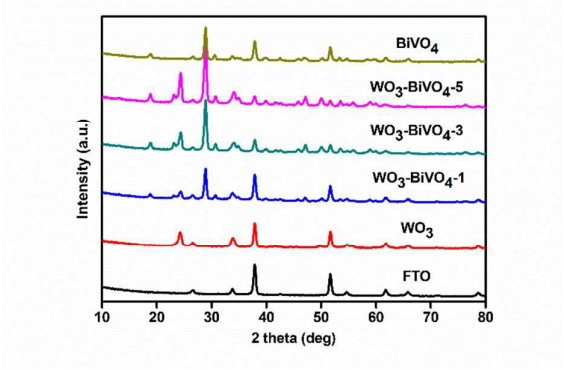

Fig.1 X-Ray diffraction patterns of FTO, bare WO_3, WO_3-$BiVO_4$-n (n=1, 3, 5) and bare $BiVO_4$ sample.

The surface morphologies of the multilayer heterojunctions were presented in Fig.2. Bare WO_3, bare $BiVO_4$ and WO_3-$BiVO_4$-5 show similar porous morphology but smaller grain sizes compared to that reported by Jae Sung Lee et al.[30] This could corresponding to different binder used for spin-coating (PVA in our work and polyethyleneimine (PEI) in Lee's work). For the bare WO_3 film, the porous network with 50 nm grain size provides a large number of reaction sites and short distance for holes to travel to the surface[41, 42]. For bare $BiVO_4$ film, larger grain size (~ 150 nm) was observed. There is no significant grain size change for $BiVO_4$ layer in the WO_3-$BiVO_4$-5 film as shown in Fig.2c. The thickness of WO_3-$BiVO_4$-5 film is ca. 324 nm as shown in Fig.2d. As five cycles of coating-anneal steps was conducted in the preparation of WO_3-$BiVO_4$-5 film, the thickness of a single WO_3/$BiVO_4$ heterojunction is calculated to be ca. 65 nm by dividing 324 nm with 5. All the surface morphologies of multilayer heterojunctions have little difference since the same synthetic condition except layer number was prepared.

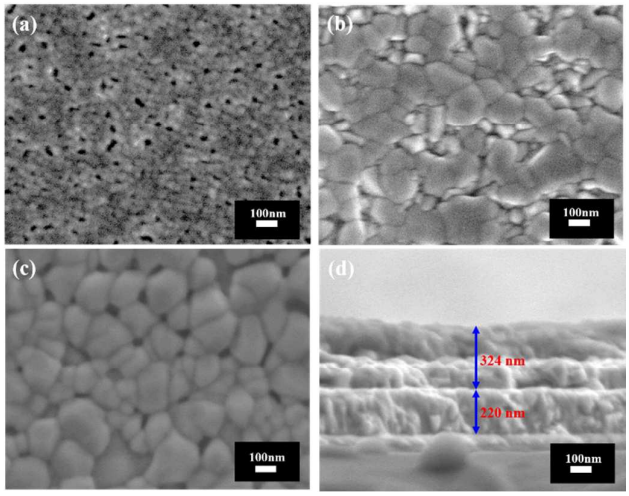

Fig.2 SEM images of different samples (a) bare WO_3; (b) bare $BiVO_4$; (c) WO_3-$BiVO_4$-5; (d) cross-sectional views of sample WO_3-$BiVO_4$-5

The distribution of Bi/W atomic ratio as a function of etching time for multilayers heterojunctions (taking WO_3-$BiVO_4$-3 (F) as a representative sample) was illustrated by Fig.3. The etching ratio was controled at 0.1nm/s. As etching time increasing, obvious Bi/W ratio changing was found along the different layers, confirming a successful fabrication of multilayer heterojunction. The thickness of a single WO_3/$BiVO_4$ bi-layer is determined to be 66 nm by averaging 64 nm with 68 nm, which is consistent with the SEM result.

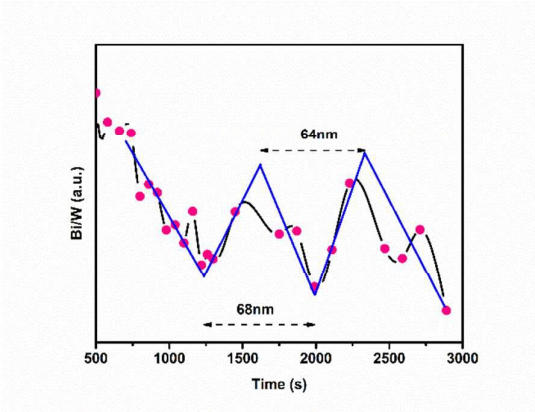

Fig.3 XPS etching profile of sample WO_3-$BiVO_4$-3 (F)

3.2 optical properties

The optical behavior of heterojunction photoelectrodes were investigated by UV-Vis absorbance spectra as shown in Fig.S2. The onset of light absorption by the bare WO_3 photoelectrode started at 450 nm (Fig.S2a) in correspondence with its band gap energy of 2.76 eV (Fig.S2b). The bare $BiVO_4$ photoelectrode exhibited an absorption edge at 500 nm, commensurate with a band gap of 2.56 eV. For the fingers-crossing heterojunction photoelectrodes, the absorption edges were between at 450 nm and 500 nm. All the absorbance intensity increased with layer number increasing while the band absorption edges, which closely resemble the bandgap of $BiVO_4$, were identical. Similar absorbance spectra were observed for sandwich heterojunction photoelectrodes.

3.3 PEC performance of multilayer heterojunction photoelectrodes

Photocurrent densities were measured in a three electrodes system. It was found that the photocurrents of both fingers-crossing heterojunctions and sandwich heterojunctions (Fig.4) increased first and then decreased with layer number increasing. In the label of the curves, number 1 to 5 indicates layer number of WO_3-$BiVO_4$ bi-layers, F stands for fingers-crossing heterojunction and S stands for sandwich heterojunction. The maximum photocurrent densities for the samples of WO_3-$BiVO_4$-3(F) and WO_3-$BiVO_4$-3(S) were 1.08 mA /cm^2 and 1.05 mA /cm^2 at 1.60 V_{RHE}, respectively. This can be explained as the number of photogenerated carriers gradually achieved saturated with the layer number increasing while the internal recombination started to play a major role when the layer number is higher than 3. At the rising part of the curve, the increase of layer number lead to higher light absorption and thus higher photocurrent. While at the dropping part of

the curve, further increase of layer number increased the distance for charge transport and thus gave a higher recombination rate. The trade-off between the light absorption and charge transport distance was also reported by Kazuhiro Sayama et al.[43]

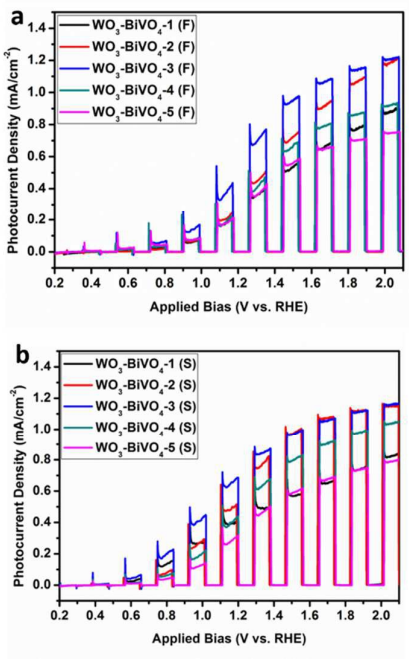

Fig.4 Current density–potential curves under chopped simulated AM 1.5G light irradiation of (a) fingers-crossing heterojunctions and (b) sandwich heterojunctions with different number of bi-layers.

Fig.5a shows the photocurrent densities of the three bi-layers heterojunction photoelectrodes of WO_3-$BiVO_4$-3(F) and WO_3-$BiVO_4$-3(S). As applied bias increasing, a faster photocurrent density increase was observed for sample WO_3-$BiVO_4$-3(S). The photocurrent density of WO_3-$BiVO_4$-3(S) was greater than that of WO_3-$BiVO_4$-3(F), approximately 1.1 times at 1.4 V_{RHE}. This is ascribed to the presence of nodes reduced the performance of separating photogenerated electron-hole pairs. While with applied bias increased, close saturated photocurrents were obtain for both samples. This could be ascribed to the larger applied bias promoted charge carrier separation[20] and the influence of WO_3 and $BiVO_4$ node on photocurrent was reduced.

In order to compare the photoactive wavelength regime for for various photoelectrodes and make a quantitative correlation between fingers-crossing heterojunction and sandwich heterojunction, incident photon to conversion efficiency measurements were conducted under 1.4 V_{RHE} in 0.5 M Na_2SO_4 aqueous solution. The IPCE can be expressed as[37]:

$$IPCE = \frac{1240I}{\lambda J_{light}} \quad (1)$$

Where I is the photocurrent density, λ is the incident light wavelength, and J_{light} is the measured irradiance. Fig.5b shows the comparison of IPCE for WO_3-$BiVO_4$-3(F) and WO_3-$BiVO_4$-3(S). The IPCE characteristics show similar dependence on wavelength with the optical band onsets at 510 nm. The highest efficiency 31% at 400 nm for WO_3-$BiVO_4$-3(S) was approximately 1.41 times to 22% at 400 nm for WO_3-$BiVO_4$-3(F). This improvement is much higher than that under white light illumination which possible due to the low light intensity.

To have a better insight into the efficient water oxidation, the charge separation efficiency ($\eta_{separation}$) and injection efficiency ($\eta_{injection}$) test were conducted in the 0.5 M Na_2SO_4 electrolyte containing 0.5 M H_2O_2. $\eta_{separation}$ or $\eta_{injection}$ are the fractions of photogenerated holes that do not recombine with electrons in the bulk or at surface traps, respectively. The relationship of water splitting photocurrent (J_{H2O}), photon absorption photocurrent density ($J_{absorbed}$), $\eta_{separation}$ and $\eta_{injection}$ can be expressed as follows[44, 45]:

$$J_{H_2O} = J_{absorbed} \times \eta_{separation} \times \eta_{injection} \quad (2)$$

H_2O_2 as a hole scavenger in the electrolyte makes the $\eta_{injection}$ becomes 100% ($\eta_{injection}$=1). So, the photocurrent measured with H_2O_2 in the electrolyte (J_{H2O2}) can be expressed as follows:

$$J_{H_2O_2} = J_{absorbed} \times \eta_{separation} \quad (3)$$

Hence, the $\eta_{separation}$ and $\eta_{injection}$ are achieved by dividing J_{H2O2} by $J_{absorbed}$ and dividing J_{H2O} by J_{H2O2}, respectively. The details can be expressed as follows:

$$\eta_{separation} = J_{H_2O_2}/J_{absorbed} \quad (4)$$

$$\eta_{injection} = J_{H_2O}/J_{H_2O_2} \quad (5)$$

By measuring the light absorption of the sample WO_3-$BiVO_4$-3 and integrating it with respect to the AM 1.5G solar spectrum, $J_{absorbed}$ was calculated to be 6.17 mA/cm^2. Fig.5c and Fig.5d present the charge separation efficiency and injection efficiency, respectively. The WO_3-$BiVO_4$-3(F) and WO_3-$BiVO_4$-3(S) show the same $\eta_{separation}$ as applied bias increasing indicates that the nodes show no effect on the recombination between electrons and holes in the bulk. While the obtained different $\eta_{injection}$ between WO_3-$BiVO_4$-3(F) and WO_3-$BiVO_4$-3(S) suggested that nodes influenced the recombination behaviour at the surface. At a low applied bias of 0.6 V_{RHE}, 7.6% and 45.7% were achieved for the WO_3-$BiVO_4$-3(F) and WO_3-$BiVO_4$-3(S) respectively. However, at a high bias of 1.85 V_{RHE}, a same $\eta_{injection}$ (97.2%) was achieved for both the films. These results can be explained as that the sandwich type structure of WO_3/$BiVO_4$ multi-layer heterojunction possess a better surface reaction activity, while for the finger-crossing structure, a higher applied bias is required to achieve an efficient surface reaction.

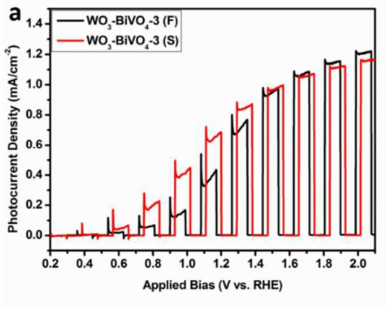

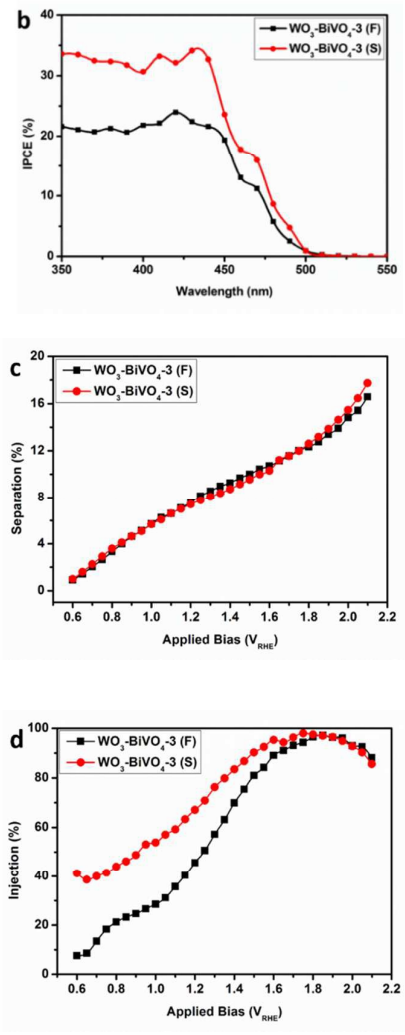

Fig.5 (a) Current density–potential curves under chopped simulated AM 1.5G light irradiation, (b) IPCE performance, (c) charge separation efficiency and (d) charge injection efficiency of sample WO_3-$BiVO_4$-3 (F) and WO_3-$BiVO_4$-3 (S).

Fig.6 shows the relationship of layer number and photocurrent difference value (DV) between samples WO_3-$BiVO_4$-n (F) and samples WO_3-$BiVO_4$-n (S) at 1.1 V_{RHE}. The photocurrent difference is the value obtained by deducting photocurrent of sandwich samples with fingers-crossing samples at 1.1 V_{RHE}. With layer number increasing, the photocurrent difference increased first then decreased and got its maximum value 0.322 mA/cm^2 at three bi-layers. When the layer number is below 3, the photogenerated holes are easily transfer to the electrode/electrolyte interface to oxidize water as the carrier diffusion length of $BiVO_4$ is ca. 70nm[40]. When the layer number is over 3, the thick thickness of films inhibit the hole transfer and reduce the photocurrent.

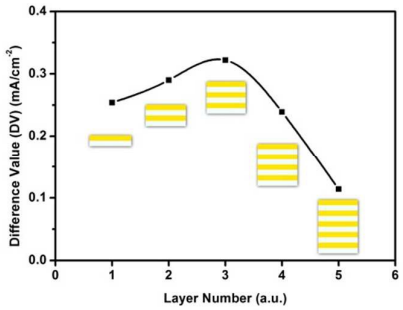

Fig.6 the relationship of layer number and photocurrent difference value (DV) between samples WO_3-$BiVO_4$-n (F) and WO_3-$BiVO_4$-n (S) at 1.1 V_{RHE}.

In order to investigate the influence of thickness of each layer on their photocurrent densities, we kept bi-layers number of heterojunctions at two and adjust the thickness of each layer by changing the spin-coating circle number for each layer. The thickness of each layer was controlled simultaneously with the same spin-coating circle number. The samples were labelled as Double-n (n=1, 2, 3, 4, 5, n indicates spin-coating circle number). Fig.7a shows the photocurrent density of fingers-crossing heterojunction (Double-n (F)) and sandwich heterojunction (Double-n (S)) at applied bias of 1.2 V_{RHE}. As layer thickness increasing, photocurrent densities for both structures were decreased. This can be interpreted as the enhancement of the recombination with the thickness of each layer thickness increasing. The photocurrent density decay with increase thickness of each layer for the sandwich heterojunction is slower when compared to that of the fingers-crossing heterojunction. 76% of the photocurrent (at 1.2 V_{RHE}) is remained for sandwich heterojunction while only 31% of photocurrent is left for that of fingers-crossing heterojunction. This can be due to a higher recombination rate of photogenerated electron-hole pairs with the presence of nodes in the fingers-crossing heterojunction. These results mean the thin thickness of each layer could reduce the effects of nodes. When reduced the concentration of precursors to half (0.0625 M), the $BiVO_4$ layer cannot cover all the FTO substrate (Fig.S3). Thus, the optimum thickness of each layer is controlled at one spin-coating cycle with a single thickness of WO_3/$BiVO_4$ heterojunction is ca. 65 nm. It is found that the photocurrent performances of all fingers-crossing heterojunction are worse than that of sandwich heterojunction with same layer number and thickness. Fig.7b shows the photocurrents of the fingers-crossing heterojunction and sandwich heterojunction of Double-5. The photocurrent density of the Double-5 (S) is 2.8 times to that of Double-5 (F) at 1.6 V_{RHE}.

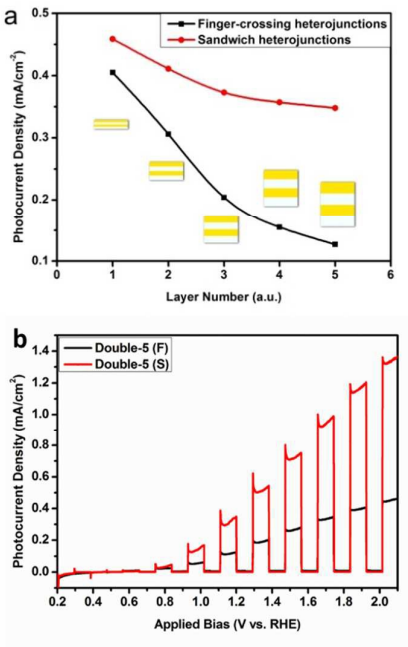

Fig.7 The relationship of layer thickness and photocurrent performance (a) photocurrent densities of heterojunctions at applied bias of 1.2 V_{RHE}; (b) comparison of photocurrent performances of Double-5 (F) and Double-5 (S)

In order to study the effects of WO_3 node and $BiVO_4$ node toward flat band potential, impedance measurements conducted at different frequencies (1, 2, 5, 10 kHz) on prepared samples in 0.5 M Na_2SO_4 electrolyte in the dark allowed the construction of Mott-Schottky plots based on the following equation 2:[30]

$$\frac{1}{C_{sc}^2} = \frac{2}{e\varepsilon\varepsilon_0 N_d} \cdot (E - E_{fb} - \frac{kT}{e}) \qquad (6)$$

Where C_{SC} is the space charge capacitance in *F*; *e* is the electronic charge in C; ε is the dielectric constant of the semiconductor; ε_0 is the permittivity of free space; N_d is the carrier density in cm^{-3}; *E* is the applied bias in V; E_{fb} is the flat band potential in V; *k* is the Boltzmann constant; *T* is the temperature in K.

The x intercept and the slope of the linear region in plot of C_{SC}^{-2} versus *E* are usually used to determine the flat band potential and the density of carriers. The plot of impedance versus frequency (Fig. S4) was plotted to check the validity of the Mott-Schottky results. As shown in Fig.8, the flat band potential values of WO_3-$BiVO_4$-5(F) and WO_3-$BiVO_4$-5(S) were determined to be 0.55 V_{RHE} and 0.08 V_{RHE}, respectively, both values are between that of pure WO_3 and $BiVO_4$ (1.14 V_{RHE} and 0.01 V_{RHE}, respectively) and are similar to reported results[30, 46]. It can be found that the existence of nodes have effects on the flat band potential and the density of carriers. The sandwich heterojunction possess a more negative flat band potential than fingers-crossing heterojunction. From the slope it was found that all the deposited films possessed a nature of n-type semiconductor. For an n-type semiconductors, a smaller slope value of WO_3-$BiVO_4$-5(S) than that of WO_3-$BiVO_4$-5(F) indicates the WO_3-$BiVO_4$-5(S) have a larger density of carriers compared to the latter.

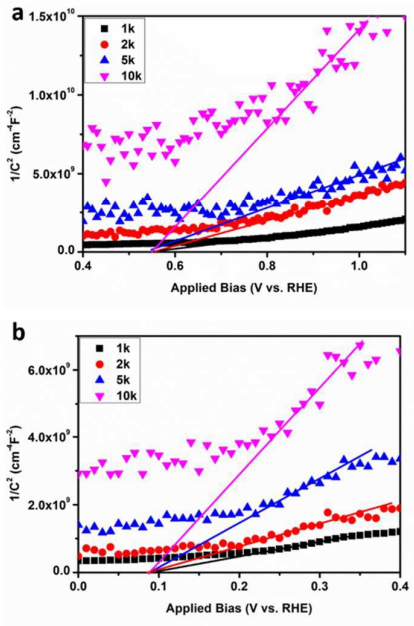

Fig.8 Mott–Schottky plots of (a) WO_3-$BiVO_4$-5(F) and (b) WO_3-$BiVO_4$-5(S) at different frequencies.

The electrochemical impedance spectroscopy (EIS) was also carried out under front illumination at 1.1 V_{RHE} to further compare the charge transfer properties between fingers-crossing and sandwich heterojunction. The Nyquist plots of EIS results were shown in Fig.9. The circle dots in the plot represent the experimental data, and the solid lines represent the fitting curve using the equivalent circuit model shown inside the plot. In the equivalent Randle circuit, R_s is the solution resistance, Q_1 and Q_2 are the constant phase elements (CPE) which stand for the electrolyte-photoelectrode interface and WO_3-$BiVO_4$ interface. The R_{ct1} and R_{ct2} are the charge transfer resistances across the interfaces of electrolyte-photoelectrode and WO_3-$BiVO_4$. The parameters extracted from the equivalent circuit fitting were shown in Table 1. The semicircle at high frequency end in the Nyquist plot corresponds to the charge transfer resistance (R_{ct})[4, 47]. As can be seen in Fig.9, sandwich heterojunction WO_3-$BiVO_4$-3(S) shows a smaller R_{ct2} and Q_2 than WO_3-$BiVO_4$-3(F), presumably resulted from the absence of WO_3 node and $BiVO_4$ node. The smaller R_{ct2} and Q_2 of WO_3-$BiVO_4$-3(S) than WO_3-$BiVO_4$-3(F) indicates that the sandwich heterojunction is a structure more favourable for charge transfer than fingers-crossing heterojunction. While the extracted parameters of R_{ct1} and Q_1 for fingers-crossing and sandwich heterojunctions are close indicating that both WO_3 node and $BiVO_4$ node have little effect on the electron transport at the interface of semiconductor/electrolyte.

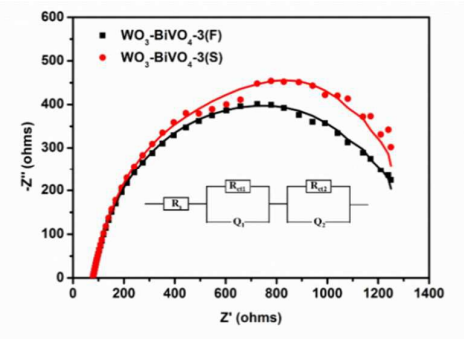

Fig.9 Nyquist plots of sample WO_3-$BiVO_4$-3(F) and WO_3-$BiVO_4$-3(S)

Table 1 simulated parameters of equivalent circuit model

Samples	R_s (Ω)	R_{ct1} (kΩ)	Q_1		R_{ct2} (kΩ)	Q_2	
			$Y_{01}(10^{-5})$	n_1		$Y_{02}(10^{-5})$	n_2
WO_3-$BiVO_4$-3(F)	78.19	1.01	6.68	0.80	3.03	2.68	0.89
WO_3-$BiVO_4$-3(S)	80.12	1.32	5.36	0.74	0.19	1.89	1.00

For the WO_3-$BiVO_4$ heterojunction in the Na_2SO_4 solution the energy band positions of $BiVO_4$ (V_{CB}=0.02 eV, V_{VB}=2.53 eV, V vs NHE) and WO_3 (V_{CB}=0.41 eV, V_{VB}=2.77 eV, V vs NHE) were reported by Lee[27]. It was widely accepted that the bottoms of the conduction bands in several n-type semiconductors are more negative by 0.1 V ~0.3 V than the flat band potential[37, 48]. Based on band positions, optical band gap energies and the experimental results discussed above, we propose a band structure model for our two different types of multilayer heterojunctions as shown in Scheme 2. We take $BiVO_4$/WO_3/$BiVO_4$ as a one cycle junction (shown in Scheme 2c) and discuss the band structures of each outermost cycle junction (shown in Scheme 2a and Scheme 2b). Both the conduction band and valence band edge of $BiVO_4$ are more negative than the corresponding band edges of WO_3. This band structure facilitates the injection of photogenerated electrodes from the conduction band of $BiVO_4$ to that of WO_3. For the heterojunctions under light irradiation, symmetrical space charge fields E_{n1} and E_{n2} should generate two voltages (ΔV_{n1} and ΔV_{n2}) in opposite directions[49]. For the fingers-crossing heterojunction, the WO_3 node connects all the WO_3 fingers resulting in equipotential within all WO_3 layers. The same situation should be expected in all $BiVO_4$ layers. The equipotential connections contribute to the same amplitude of ΔV_{n1} and ΔV_{n2}. This indicates that the total voltage difference (ΔV_n) in one cycle junction should be zero (ΔV_{n1}+ ΔV_{n2}=0) at the adjacent junctions. However, underlaying junctions will generate smaller photovoltage (ΔV_n) as less light was absorbed. While the case for the sandwich heterojunctions without WO_3 or $BiVO_4$ node is different. With absence of equipotential connection, there is additional Fermi level drop in the outer $BiVO_4$ layer induced by electrons flowed to the double layer across the $BiVO_4$/electrolyte. Thus, the space charge region at $BiVO_4$/WO_3 was strengthened while that at WO_3/$BiVO_4$ was weakened, resulting in $\Delta V_{n1} < \Delta V_{n2}$. As to the next $BiVO_4$/WO_3/$BiVO_4$ cycle, the space charge region of WO_3/$BiVO_4$ was weakened because that of $BiVO_4$/WO_3 in the previous cycle was strengthened. With repeat of $BiVO_4$/WO_3/$BiVO_4$ cycles, the conduction band edges of semiconductors in each layer in sandwich heterojunction gradually shifted to negative values, as shown in Scheme 2b. That is why the flat-band potential of sandwich heterojunction is more negative compared to that of fingers-crossing heterojunction, and this flat-band potential shift is beneficial for charge separation and thus the photoelectrochemical activity.

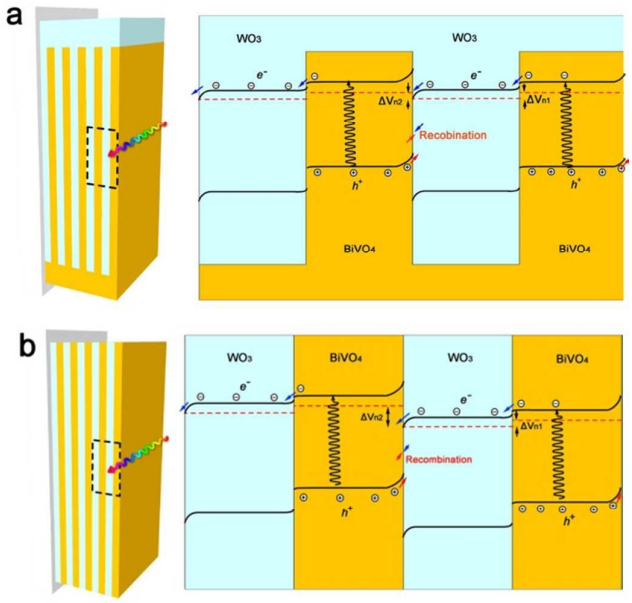

Scheme 2 Schematic illustration of interfacial band edge structure within (a) two cycle junctions of fingers-crossing heterojunction, (b) two cycle junctions of sandwich heterojunction

4 Conclusions

Fingers-crossing heterojunction and sandwich heterojunction WO_3/$BiVO_4$ photoelectrodes were fabricated on FTO substrates. Both the as prepared WO_3 layer and $BiVO_4$ layer possess monoclinic phase. The layer number and layer thickness influences on the PEC performance were investigated and optimal layer number was found as 3 layers and the best thickness for each layer was the thinnest thickness used. It is also found that the flat band potential in the sandwich heterojunction shifted negative compared to fingers-crossing one and an enhancement of PEC performance for hydrogen production was observed especially when applied with low bias. This work compared two different types of heterojunction and showed that the PEC property is sensitive to their junction types. With regard to further improve the PEC performance of heterojunctions, optimizing structure the electrode remains a promising approach, and it can also inspire ideas for investigating other heterostructures.

Acknowledgements

This work was supported by the National Natural Science Foun dation of China (No.51202186).

Notes and references

1. H. W. Jeong, T. H. Jeon, J. S. Jang, W. Choi and H. Park, *J. Phys. Chem. C*, 2013, **117**, 9104-9112.
2. K. Zhang and L. Guo, *Catal. Sci. Technol.*, 2013, **3**, 1672.
3. D. Eisenberg, H. S. Ahn and A. J. Bard, *J. Am. Chem. Soc.*, 2014, **136**, 14011-14014.
4. X. Fu, M. Xie, P. Luan and L. Jing, *Appl. Mater. Inter.*, 2014, **6**, 18550-18557.
5. P. Chatchai, A. Y. Nosaka and Y. Nosaka, *Electrochim. Acta*, 2013, **94**, 314-319.
6. F. E. Osterloh, *Chem. Soc. Rev.*, 2013, **42**, 2294-2320.
7. R. Daghrir, P. Drogui and D. Robert, *Ind. Eng. Chem. Res.*, 2013, **52**, 3581-3599.
8. K. Sivula, F. L. Formal and M. Grätzel, *ChemSusChem*, 2011, **4**, 432-449.
9. T. Hisatomi, J. Kubota and K. Domen, *Chem. Soc. Rev.*, 2014, **43**, 7520-7535.
10. J. Su, L. Guo, N. Bao and C. A. Grimes, *Nano Lett.*, 2011, **11**, 1928-1933.
11. M. T. Mayer, C. Du and D. Wang, *J. Am. Chem. Soc.*, 2012, **134**, 12406-12409.
12. S. Liu, N. Zhang, Z. Tang and Y. Xu, *Appl. Mater. Inter.*, 2012, **4**, 6378-6385.
13. Y. Tak, S. J. Hong, J. S. Lee and K. Yong, *J. Mater. Chem.*, 2009, **19**, 5945.
14. S. Ho-Kimura, S. J. A. Moniz, A. D. Handoko and J. Tang, *J. Mater. Chem. A*, 2014, **2**, 3948.
15. S. J. A. Moniz, J. Zhu and J. Tang, *Adv. Energy. Mater.*, 2014, **4**.
16. K. Sivula, F. L. Formal and M. Grätzel, *Chem. Mater.*, 2009, **21**, 2862-2867.
17. S. Shenawi-Khalil, V. Uvarov, S. Fronton, I. Popov and Y. Sasson, *J. Phys. Chem. C*, 2012, **116**, 11004-11012.
18. R. Saito, Y. Miseki and K. Sayama, *Chem. Commun.*, 2012, **48**, 3833-3835.
19. H. Yoon, M. G. Mali, J. Y. Choi, M.-w. Kim, S. K. Choi, H. Park, S. S. Al-Deyab, M. T. Swihart, A. L. Yarin and S. S. Yoon, *Langmuir*, 2015, **31**, 3727-3737.
20. M. Long, W. Cai and H. Kisch, *J. Phys. Chem. C*, 2008, **112**, 548-554.
21. Y. H. Ng, A. Iwase, A. Kudo and R. Amal, *J. Phys. Chem. Lett.*, 2010, **1**, 2607.
22. R. Saito, Y. Miseki and K. Sayama, *J. Photochem. Photobiol., A*, 2013, **258**, 51-60.
23. Y. Park, K. J. McDonald and K. S. Choi, *Chem. Soc. Rev.*, 2013, **42**, 2321-2337.
24. M. Zhong, T. Hisatomi, Y. Kuang, J. Zhao, M. Liu, A. Iwase, Q. Jia, H. Nishiyama, T. Minegishi, M. Nakabayashi, N. Shibata, R. Niishiro, C. Katayama, H. Shibano, M. Katayama, A. Kudo, T. Yamada and K. Domen, *Journal of the American Chemical Society*, 2015, **137**, 5053-5060.
25. S. K. Cho, H. S. Park, H. C. Lee, K. M. Nam and A. J. Bard, *J. Phys. Chem. C*, 2013, **117**, 23048-23056.
26. N. F. Fatwa F. Abdi, Ali Dabirian and Roel van de Krol, *Mater. Res. Soc. Symp. Proc.*, 2012, **1446**, 7-12.
27. M. T. McDowell, M. F. Lichterman, J. M. Spurgeon, S. Hu, I. D. Sharp, B. S. Brunschwig and N. S. Lewis, *J. Phys. Chem. C*, 2014, **118**, 19618-19624.
28. C. A. Bignozzi, S. Caramori, V. Cristino, R. Argazzi, L. Meda and A. Tacca, *Chem. Soc. Rev.*, 2013, **42**, 2228-2246.
29. S. K. Pilli, R. Janarthanan, T. G. Deutsch, T. E. Furtak, L. D. Brown, J. A. Turner and A. M. Herring, *Phys. Chem. Chem. Phys.*, 2013, **15**, 14723-14728.
30. S. J. Hong, S. Lee, J. S. Jang and J. S. Lee, *Energy Environ. Sci.*, 2011, **4**, 1781-1787.
31. K. Zhang, X. J. Shi, J. K. Kim and J. H. Park, *Phys. Chem. Chem. Phys.*, 2012, **14**, 11119-11124.
32. L. Xia, J. Bai, J. Li, Q. Zeng, X. Li and B. Zhou, *Appl. Catal., B*, 2016, **183**, 224-230.
33. P. M. Rao, L. Cai, C. Liu, I. S. Cho, C. H. Lee, J. M. Weisse, P. Yang and X. Zheng, *Nano Lett.*, 2014, **14**, 1099-1105.
34. Y. Pihosh, I. Turkevych, K. Mawatari, J. Uemura, Y. Kazoe, S. Kosar, K. Makita, T. Sugaya, T. Matsui, D. Fujita, M. Tosa, M. Kondo and T. Kitamori, *Scientific reports*, 2015, **5**, 11141.
35. Y. Pihosh, I. Turkevych, K. Mawatari, T. Asai, T. Hisatomi, J. Uemura, M. Tosa, K. Shimamura, J. Kubota, K. Domen and T. Kitamori, *Small*, 2014, **10**, 3692-3699.
36. X. Shi, I. Y. Choi, K. Zhang, J. Kwon, D. Y. Kim, J. K. Lee, S. H. Oh, J. K. Kim and J. H. Park, *Nat Commun*, 2014, **5**, 4775.
37. T. W. Kim and K. S. Choi, *Science*, 2014, **343**, 990-994.
38. I. Grigioni, K. G. Stamplecoskie, E. Selli and P. V. Kamat, *J. Phys. Chem. C*, 2015, **119**, 20792-20800.
39. J. Su, X. Feng, J. D. Sloppy, L. Guo and C. A. Grimes, *Nano Lett.*, 2011, **11**, 203-208.
40. F. F. Abdi, T. J. Savenije, M. M. May, B. Dam and R. van de Krol, *J. Phys. Chem. Lett.*, 2013, **4**, 2752-2757.
41. S. J. Hong, H. c. Jun, P. H. Borse and J. S. Lee, *Int. J. Hydrogen Energy*, 2009, **34**, 3234.
42. M. U. Clara Santato, and Jan Augustynski, *J. Phys. Chem. B*, 2001, **105**, 936-940.
43. I. Fujimoto, N. Wang, R. Saito, Y. Miseki, T. Gunji and K. Sayama, *Int. J. Hydrogen Energy*, 2014, **39**, 2454-2461.
44. H. Dotan, K. Sivula, M. Grätzel, A. Rothschild and S. C. Warren, *Energy Environ. Sci.*, 2011, **4**, 958-964.
45. J. H. Kim, Y. J. Jang, J. H. Kim, J. W. Jang, S. H. Choi and J. S. Lee, *Nanoscale*, 2015, **7**, 19144-19151.
46. M. Li, L. Zhao and L. Guo, *Int. J. Hydrogen Energy*, 2010, **35**, 7127-7133.
47. L. Zhang, E. Reisner and J. J. Baumberg, *Energy Environ. Sci.*, 2014, **7**, 1402-1408.
48. P. Bornoz, F. F. Abdi, S. D. Tilley, B. Dam, R. van de Krol, M. Graetzel and K. Sivula, *J. Phys. Chem. C*, 2014, **118**, 16959-16966.
49. J. Cao, J. Xing, Y. Zhang, H. Tong, Y. Bi, T. Kako, M. Takeguchi and J. Ye, *Langmuir*, 2013, **29**, 3116-3124.

Table of contents entry for

Comparison of Sandwich and Fingers-crossing type $WO_3/BiVO_4$ Multilayer Heterojunctions for Photoelectrochemical Water Oxidation

Cong Liu, Jinzhan Su* and Liejin Guo

International Research Center for Renewable Energy, State Key Laboratory of Multiphase Flow, Xi'an Jiaotong University, Xi'an, Shaanxi 710049, P. R. China

E-mail: j.su@mail.xjtu.edu.cn

Text: Sandwich and Finger-crossing type $WO_3/BiVO_4$ Multilayer Heterojunctions were deposited to investigate the influence of junction structure on their PEC photoelectrochemical performances.

Colour graphic: